Optics Letters

Versatile multimodal modality based on Brillouin light scattering and the photoacoustic effect

Chenjun Shi,[1,†] Yan Yan,[2,†] Mohammad Mehrmohammadi,[2,3,4] and Jitao Zhang[1,*]

[1]Department of Biomedical Engineering, College of Engineering, Wayne State University, Detroit, Michigan 48202, USA
[2]Department of Imaging Science, School of Medicine and Dentistry, University of Rochester Medical Center, Rochester, New York 14642, USA
[3]Department of Biomedical Engineering, Hajim School of Engineering and Applied Sciences, University of Rochester, Rochester, New York 14642, USA
[4]mohammad_mehr@urmc.rochester.edu
[†]These authors contributed equally.
[*]zhang4@wayne.edu

Received 15 May 2023; revised 1 June 2023; accepted 2 June 2023; posted 6 June 2023; published 20 June 2023

Multimodal optical techniques are useful for the comprehensive characterization of material properties. In this work, we developed a new, to the best of our knowledge, multimodal technology that can simultaneously measure a subset of mechanical, optical, and acoustical properties of the sample and is based on the integration of Brillouin (Br) and photoacoustic (PA) microscopy. The proposed technique can acquire co-registered Br and PA signals from the sample. Importantly, using synergistic measurements of the speed of sound and Brillouin shift, the modality offers a new approach to quantifying the optical refractive index, which is a fundamental property of a material and is not accessible by either technique individually. As a proof of concept, we demonstrated the feasibility of integrating the two modalities and acquired the colocalized Br and time-resolved PA signals in a synthetic phantom made out of kerosene and $CuSO_4$ aqueous solution. In addition, we measured the refractive index values of saline solutions and validated the result. Comparison with previously reported data showed a relative error of 0.3%. This further allowed us to directly quantify the longitudinal modulus of the sample with the colocalized Brillouin shift. While the scope of the current work is limited to introducing the combined Br-PA setup for the first time, we envision that this multimodal modality could open a new path for the multi-parametric analysis of material properties.

https://doi.org/10.1364/OL.495361

Photoacoustic (PA) microscopy is a rapidly growing modality with the ability to acquire high-contrast functional and molecular images of samples at relatively large depths compared to conventional optical techniques [1–3]. In PA microscopy, the absorption of light energy in the form of short laser pulses generates acoustic waves caused by rapid thermoelastic expansion [1]. The consequent acoustic waves can be collected by acoustic detectors such as an ultrasound transducer or a hydrophone to form PA images. The amplitude of the detected PA signal represents the optical absorption and scattering properties of the material. In addition, using PA microscopy, an important acoustic property of the material, namely the speed of sound (SOS), can be obtained by calculating the time of flight (TOF) of the PA signal with prior knowledge of the physical distance between the detector and the location of the excitation beam.

Confocal Brillouin microscopy is an emerging optical modality for quantifying the mechanical properties of materials with diffraction-limit resolution [4–7]. The principle of Brillouin microscopy is based on spontaneous Brillouin scattering, where the interaction of incident light and the inherent acoustic wave from thermal fluctuation within the sample introduces a frequency shift (i.e., the Brillouin shift ω_B) into the scattered light. The Brillouin shift at 90° geometry is physically determined as $\omega_B = \sqrt{2}n/\lambda \cdot \sqrt{M'/\rho}$, where λ is the laser wavelength, n is the refractive index, ρ is the sample's density, and M' is the elastic longitudinal modulus. With a known refractive index and density, the sample's mechanical properties can be directly quantified with the Brillouin shift measured by a Brillouin spectrometer [8].

Currently, Brillouin microscopes mainly use the Brillouin shift to estimate the relative change in longitudinal modulus, with the assumption that the ratio of the refractive index and density $n/\sqrt{\rho}$ is approximately constant [5,9–13]. However, for benchmarking and comparisons across studies, direct quantification of the absolute value of the longitudinal modulus is needed, which requires the colocalized measurement of the refractive index and/or mass density of the material. Recently, two methods, dual-geometry Brillouin microscopy [14] and a multimodal modality that combines Brillouin microscopy with optical diffraction tomography [15], have been demonstrated for this purpose.

In this work, we report, for the first time to the best of our knowledge, a proof-of-concept multimodal optical modality that combines PA and Brillouin microscopy. In this hybrid modality, two laser beams are coupled into a common optical path to collect the Brillouin and time-resolved PA signals from the same spot simultaneously. Therefore, this new modality allows us to acquire the colocalized mechanical, optical, and acoustic properties of the material for comprehensive characterization. Intriguingly, using the SOS (V_S) derived from the PA signal, we

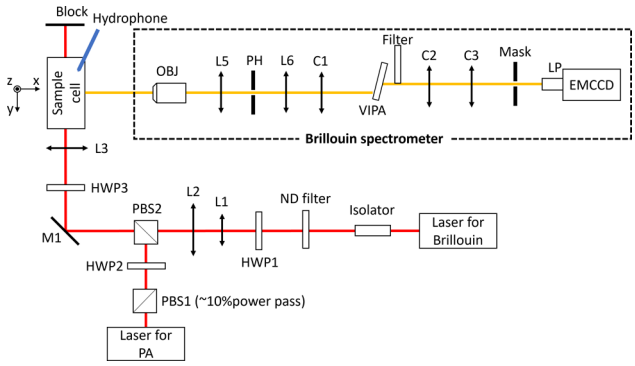

Fig. 1. Schematic of the multimodal modality based on Brillouin and PA techniques. HWP1–HWP3: half-wave plates; PBS1–PBS2: polarized beam splitter; L1–L5: lenses; OBJ: objective; PH: pinhole; C1–C3: cylindrical lenses; LP: lens pair; EMCCD: electron-multiplying charge-coupled devices.

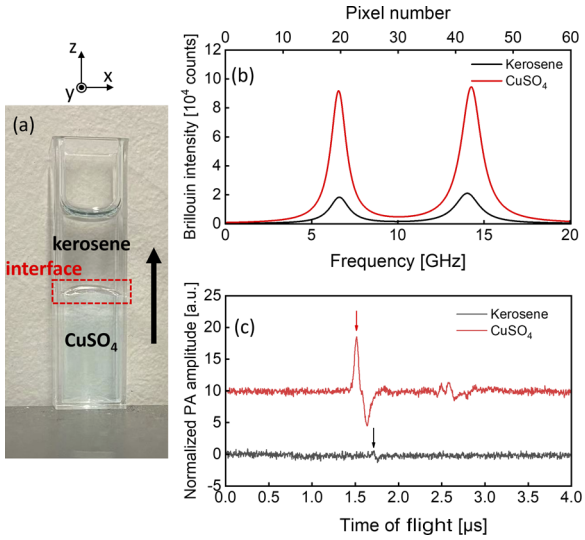

Fig. 2. Experimental sample and signals. (a) Photo of the stratified sample with the scan direction. Raw (b) Brillouin and (c) PA signals (single measurements) from $CuSO_4$ and kerosene. Arrows indicate the PA signal peak.

can directly quantify the refractive index from the measured Brillouin shift based on the relationship $V_S = \sqrt{M'/\rho} = \omega_B \lambda/\left(\sqrt{2}n\right)$, which further allows us to quantify the longitudinal modulus based on the two-substance mixture model [16–18]. It is worth highlighting that the quantitative measurement of the longitudinal modulus can only be achieved by the integrated system rather than by the Brillouin or PA modality individually.

Figure 1 shows a schematic of the multimodal PA–Brillouin microscopic system. A 780-nm continuous-wave (CW) laser (DL pro, Toptica) was used as the light source for Brillouin scattering. The laser beam first went through an isolator to avoid possible backreflection. A variable ND filter was used to adjust the output power of the laser, and a half-wave plate (HWP1) was used to adjust the polarization state of the beam to be p-polarized. Using a pair of lenses (L1, $f = 30$ mm, and L2, $f = 150$ mm), the diameter of the laser beam was expanded from 2.38 mm to 11.90 mm. After passing through the second polarized beam splitter (PBS2), the mirror M1, and a half-wave plate (HWP3), the laser beam was focused into the sample cell (a 1-cm-square cuvette) by lens L3 ($f = 75$ mm), with a focused spot of 6.26 μm. An in-house-built Brillouin spectrometer was used to collect the Brillouin signal at 90° geometry. The light source for PA excitation, emitted from a tunable nanosecond pulsed laser (OPOTEK, Phocus Mobile), was tuned to the wavelength of 780 nm and had a beam diameter of ~8 mm. Since the emitted light from the pulsed laser was randomly polarized, a polarized beam splitter (PBS1) was used first to obtain a linearly p-polarized beam. After adjusting the polarization orientation of the PA beam to s-polarization with a half-wave plate (HWP2), the PA beam was coupled into the optical path of the Brillouin beam using PBS2 and focused into the sample cell with a spot diameter of 9.31 μm. The half-wave plate (HWP3) was used to further adjust the Brillouin beam and PA beam to be s-polarized and p-polarized, respectively. Since the 90° scattering geometry is sensitive to s-polarized light but has no response to p-polarized light [19], our design can generate a strong Brillouin signal while avoiding any cross talk from the PA excitation beam.

The generated PA signal was detected by a needle hydrophone (Onda, HNP-0400, 1–20 MHz) that was inserted into the sample cell at a close distance from the focal point (~ 4 mm). Meanwhile, the Brillouin signal was measured by a virtually imaged phased array (VIPA)-based Brillouin spectrometer. Upon being collected by an objective (OBJ, 4×/0.1), the Brillouin signal passed through a confocal unit consisting of two lenses and an adjustable pinhole (L5, $f = 19$ mm; L6, $f = 80$; and PH: adjustable pinhole), through which the Brillouin signal out of the focal plane will be rejected. A cylindrical lens (C1, $f = 200$ mm) was used to couple the Brillouin beam into the VIPA etalon (FSR = 15 GHz, LightMachinery). A filter (continuous ND filter, Thorlabs) was used for apodization. The output beam of the VIPA was reshaped by the cylindrical lenses C2 ($f = 150$ mm) and C3 ($f = 75$ mm) and then projected onto the mask. A lens pair (LP, 1:1, f = 30.0 mm) was used to image the Brillouin spectrum onto an electron-multiplying charge-coupled device (EMCCD) camera (iXon, Andor). Before experiments, the spectrometer was calibrated using standard materials (i.e., water and methanol) based on an established protocol [7]. For accurate alignment of the two laser beams, several tunable iris diaphragms were placed into the beam path to check the beam location. This ensures the overlap of two beam spots at the focal plane, which can be confirmed by imaging from the side.

To evaluate the colocalization of the multimodal PA and Brillouin signals, we conducted an experiment in which a synthetic phantom [Fig. 2(a)] made of 1% copper sulfate solution ($CuSO_4$) and kerosene was scanned to acquire both PA and Brillouin profiles across the sample. For the Brillouin measurement, the laser power was 27 mW at the focal plane, and the acquisition time of the spectrometer was 50 ms. For PA measurement, the average energy of the laser pulse was 1.4 mJ at a repetition rate of 10 Hz. Figures 2(b) and 2(c) show the representative Brillouin shift and PA amplitude for $CuSO_4$ solution and kerosene, respectively. The sample cell was carried by a translation stage and was scanned manually along the z direction with a total travel range of 1.75 mm and a step size of 0.25 mm. At each position, 100 frames of Brillouin and PA signals were collected for calculating the average Brillouin shift and PA peak-to-peak amplitude. Figure 3 shows the colocalized Brillouin and PA signals across the interface of two materials. The co-registered trend for the

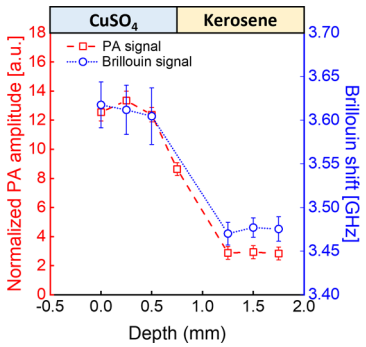

Fig. 3. Result of 1D scanning. Vertical 1D profiling of the stratified $CuSO_4$–kerosene sample based on the Brillouin shift and PA amplitude. Error bars are the standard deviations for 100 measurements.

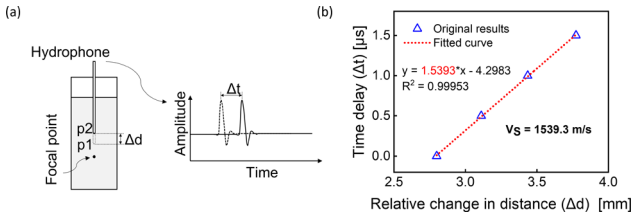

Fig. 4. Speed of sound measurement. (a) Scheme for measuring SOS. (b) Regression result from the measurement of 4.76% (w/w) saline.

Brillouin and PA curves confirms that both the Brillouin beam and the PA beam share the same focal point in the setup. At the transition zone, the decrease in the PA signal amplitude as well as the Brillouin shift is mainly due to the beam distortion caused by the curved interface of two liquids [Fig. 2(a)]. The step size is limited by the resolution of the manual translational stage.

We further explored the ability of the developed multimodal modality to directly measure the refractive index. To do so, we prepared three saline solutions: the weight/weight concentrations were 0% (de-ionized water), 4.76%, and 16.67%, respectively. The SOS (V_S) was directly measured through consecutive PA acquisitions, where the distance between the detecting hydrophone and the beam spot was changed by the preset value Δd. The time delay between the TOFs of these two consecutive PA acquisitions was measured as Δt [Fig. 4(a)], allowing the speed of sound to be calculated through $V_S = \Delta d/\Delta t$. For each sample, the transducer was moved to four positions in sequence, with a distance of 0.25 mm moved in each movement (moving accuracy: ± 0.02 mm). At each position, the PA signal was averaged 100 times, and the primary positive peak was used to quantify the arrival time. The value of V_S was then calculated from all datasets by linear regression using the least squares method [Fig. 4(b)]. Simultaneously, the Brillouin shift ω_B of the sample was calculated as described earlier. Therefore, the refractive index of the sample can be calculated by

$$n = \omega_B \lambda / \left(\sqrt{2} V_S\right), \quad (1)$$

with λ = 780 nm. For each sample, we repeated both the PA and Brillouin measurements three times, and the averaged values of the refractive index along with the standard error of the mean are

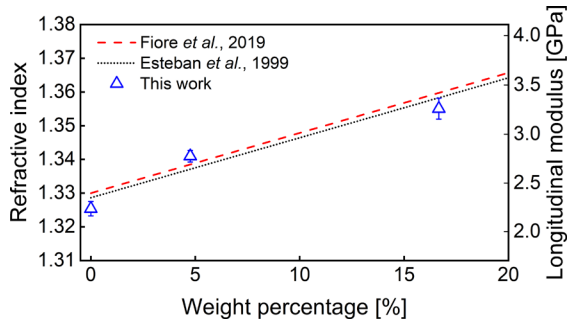

Fig. 5. Measured refractive index and longitudinal modulus values of saline solutions. Error bars represent standard errors of the mean.

Table 1. Comparison of SOS Results Calculated by Brillouin and PA Microscopy (With Standard Errors)

Weight Percentage	Brillouin Results [m/s] @3.6 GHz	PA Fitting Results [m/s] @1–20 MHz
0%	1484.02 ± 2.33	1480.80 ± 0.54
4.76%	1541.02 ± 0.60	1534.84 ± 1.87
16.67%	1675.13 ± 3.40	1669.95 ± 1.81

shown in Fig. 5. The measured refractive index was compared with the results from Fiore *et al*. (obtained using dual-geometry Brillouin spectroscopy at 532 nm) [14] and from Esteban *et al.* (obtained using a fiber-optic sensor at 780 nm) [20]. Taking the average of the literature data (Fiore's data were corrected based on water's refractive index at 780 nm and 20.7°C) as a reference, our results show a discrepancy of 0.0041 (0.31%), 0.0029 (0.22%), and 0.0042 (0.31%), respectively, suggesting good agreement. Based on the colocalized measurement of the Brillouin shift and refractive index, we also derived the longitudinal modulus of the sample (Fig. 5).

Since Brillouin microscopy probes acoustic phonons in the GHz frequency band while the PA signal is in the MHz band, possible acoustic dispersion of the sample may introduce an artifact into the measured refractive index. To estimate the acoustic dispersion, we calculated the phonon velocity at GHz, which was derived from the Brillouin measurements using the reported value of the refractive index [20], and we compared it with PA measurements at MHz. The result is summarized in Table 1, where the relative discrepancy between the two datasets is within 0.4%, indicating that the acoustic dispersion in our samples is negligible. This is also consistent with several previously reported studies in which the SOS in pure water and saline has a variation of less than 0.3% as the frequency increases from 0.5 MHz to 1.5 GHz [21–25]. In addition, linear behavior (i.e., no dispersion) of the sound wave has been found in many (bio)polymers [14], indicating the potential application of our multimodal modality in biomaterials and biological samples. For materials in which acoustic dispersion is prominent, prior knowledge of the dispersion behavior is needed for an accurate measurement of the refractive index.

Here we used a homogeneous sample to demonstrate the ability of the proof-of-concept prototype and to validate the feasibility and accuracy of refractive index measurement. In fact, the developed multimodal method can also be used for inhomogeneous conditions such as those in multi-layered samples. In

this case, the thickness of each layer can be first obtained from the Brillouin results. While keeping the PA detector still, the movement of the beam spot into different layers will introduce a time delay into the PA signal, and this delay is a function of the SOS for each layer. Therefore, the SOS of each layer can be derived by solving a set of multivariate equations. Together with the Brillouin signals, the refractive index of each layer can be measured.

While the current prototype utilizes two separate laser sources for generating Brillouin and PA signals, a single laser source could be used for both BA and Br microscopy if a pulse laser with a narrow linewidth and a nanosecond pulse width is available. In the present work, PA measurement was conducted in transmission mode, and the Brillouin signal was collected at 90° geometry. This configuration needs a cuvette to hold the sample, and the sample preparation can be adapted from existing protocols used in light-sheet microscopy. Alternatively, the setup can be modified into a reflection mode (i.e., 180° geometry) by integrating with the existing designs of inverted confocal Brillouin microscopy and PA microscopy [26], which allows easy access to biological samples prepared in a standard petri dish. Furthermore, since the densities of many biological materials can be calculated from the refractive index based on a two-substance mixture model [16–18], colocalized measurement of the refractive index and Brillouin shift will allow the direct quantification of the longitudinal modulus.

Colocalized Brillouin–PA measurement offers a unique advantage for accurate and reliable characterization of complicated biomedical processes. For instance, it can potentially simultaneously acquire biomechanical information and metabolic activities during tumorigenesis and metastasis [27], allowing a comprehensive understanding of the heterogeneity of tumor microenvironment. Broadly, the multimodal modality can provide complementary (i.e., biomechanical and optical) contrast mechanisms, which can improve the sensitivity and specificity in material and tissue characterization, leading to more accurate diagnosis [28–31].

In summary, we have proposed a versatile multimodal modality based on the combination of Brillouin microscopy and a PA system. The integrated system with a common focal point for both the Brillouin and PA beams was designed to simultaneously obtain the sample's mechanical, optical, and acoustical properties. Importantly, the integrated system provides a new way to probe the sample's refractive index, which is not accessible by either individual technique. Together, the proposed multimodal Brillouin and PA system can provide multi-parametric analysis for comprehensive material characterization.

Funding. Wayne State University; National Institute of Biomedical Imaging and Bioengineering (R01EB030058); Eunice Kennedy Shriver National Institute of Child Health and Human Development (K25HD097288).

Acknowledgments. The authors would like to thank Dr. Matthew O'Donnell from the University of Washington for discussions and valuable feedback on the sound speed measurement studies presented in this work. We also want to thank Dr. Antonio Fiore from HHMI Janelia Research Campus for providing raw data from refractive index measurements with dual-geometry Brillouin microscopy.

Disclosures. A provisional patent application related to this research has been filed by Wayne State University patent office for J.Z., C.S., Y.Y., and M. M.

Data availability. Data underlying the results presented in this paper are not publicly available at this time but may be obtained from the authors upon reasonable request.

REFERENCES

1. A. G. Bell, Science **os-1**, 130 (1880).
2. M. Xu and L. V. Wang, Rev. Sci. Instrum. **77**, 041101 (2006).
3. M. Mehrmohammadi, S. Joon Yoon, D. Yeager, and S. Y. Emelianov, Curr. Mol. Imaging **2**, 89 (2013).
4. G. Scarcelli and S. H. Yun, Nat. Photonics **2**, 39 (2008).
5. G. Scarcelli, W. J. Polacheck, H. T. Nia, K. Patel, A. J. Grodzinsky, R. D. Kamm, and S. H. Yun, Nat. Methods **12**, 1132 (2015).
6. R. Prevedel, A. Diz-Muñoz, G. Ruocco, and G. Antonacci, Nat. Methods **16**, 969 (2019).
7. J. Zhang and G. Scarcelli, Nat. Protoc. **16**, 1251 (2021).
8. J. G. Dil, Rep. Prog. Phys. **45**, 285 (1982).
9. G. Scarcelli, P. Kim, and S. H. Yun, Biophys. J. **101**, 1539 (2011).
10. G. Scarcelli, R. Pineda, and S. H. Yun, Invest. Ophthalmol. Visual Sci. **53**, 185 (2012).
11. G. Antonacci and S. Braakman, Sci. Rep. **6**, 37217 (2016).
12. J. Zhang, R. Raghunathan, J. Rippy, C. Wu, R. H. Finnell, K. V. Larin, and G. Scarcelli, Birth Defects Res. **111**, 991 (2019).
13. J. Zhang, F. Alisafaei, M. Nikolić, X. A. Nou, H. Kim, V. B. Shenoy, and G. Scarcelli, Small **16**, 1907688 (2020).
14. A. Fiore, C. Bevilacqua, and G. Scarcelli, Phys. Rev. Lett. **122**, 103901 (2019).
15. R. Schlüßler, K. Kim, M. Nötzel, A. Taubenberger, S. Abuhattum, T. Beck, P. Müller, S. Maharana, G. Cojoc, and S. Girardo, eLife **11**, e68490 (2022).
16. R. Barer, K. F. A. Ross, and S. Tkaczyk, Nature **171**, 720 (1953).
17. M. Schürmann, J. Scholze, P. Müller, J. Guck, and C. J. Chan, J. Biophotonics **9**, 1068 (2016).
18. M. Bailey, M. Alunni-Cardinali, N. Correa, S. Caponi, T. Holsgrove, H. Barr, N. Stone, C. P. Winlove, D. Fioretto, and F. Palombo, Sci. Adv. **6**, eabc1937 (2020).
19. R. W. Boyd, Nonlinear optics (Academic press, 2020).
20. O. Esteban, M. Cruz-Navarrete, A. González-Cano, and E. Bernabeu, Appl. Opt. **38**, 5267 (1999).
21. C. L. O'Connor and J. P. Schlupf, J. Chem. Phys. **47**, 31 (1967).
22. V. A. Del Grosso and C. W. Mader, J. Acoust. Soc. Am. **52**, 1442 (1972).
23. P.-K. Choi and K. Takagi, Jpn. J. Appl. Phys. **22**, 890 (1983).
24. K. i. Fujii and R. Masui, J. Acoust. Soc. Am. **93**, 276 (1993).
25. D. Liu, J. Xu, R. Li, R. Dai, and W. Gong, Opt. Commun. **203**, 335 (2002).
26. J. Yao and L. V. Wang, Laser Photonics Rev. **7**, 758 (2013).
27. D. Hanahan and R. A. Weinberg, Cell **144**, 646 (2011).
28. Y. Yan, N. Gomez-Lopez, M. Basij, A. V. Shahvari, F. Vadillo-Ortega, E. Hernandez-Andrade, S. S. Hassan, R. Romero, and M. MehrMohammadi, Biomed. Opt. Express **10**, 4643 (2019).
29. A. Samani, J. Bishop, C. Luginbuhl, and D. B. Plewes, Phys. Med. Biol. **48**, 2183 (2003).
30. J. Dias, V. F. Diakonis, V. P. Kankariya, S. H. Yoo, and N. M. Ziebarth, Exp. Eye Res. **116**, 58 (2013).
31. C. McAlinden, Clin. Exp. Optom. **95**, 386 (2012).